FULL PAPER

Crystalline Organic Heterostructures Engineering Based on Vanadyl Phthalocyanine and Rod-Like Conjugated Organic Semiconductors with Selected Central Groups

Lizhen Huang, Feng Zhu, Chengfang Liu, Uwe Treske, Mandy Grobosch, Hongkun Tian, Jidong Zhang, Yanhou Geng, Martin Knupfer, and Donghang Yan**

The effect of groups in conjugated molecules on films' interface morphology, electronic structure, and charge transport behavior is explored utilizing a series of crystalline organic heterostructures that are constructed by four rod-like molecules and vanadyl phthalocyanine (VOPc). The four rod-like molecules, which possess the same biphenyl endgroup but different central groups, present similar growth behavior along with different thin film structural parameters and electronic structures. The changes of the structure parameters result in diverse morphology of the VOPc/rod-like molecule heterostructure because of the different lattice mismatch. The electronic structure differences in rod-like molecules cause different interface electronic structure of the heterostructure. Under the conjunct effect of morphology and interface electronic structure, the transistors based on the crystalline heterostructures present diverse charge transport behavior and field-effect mobilities. These results provide a clue for the development of crystalline organic heterostructure engineering and tailoring overall organic device performance through molecular design in local inducing layer.

1. Introduction

Heterostructures play a vital role in organic semiconductor devices, such as organic light emitting diodes, organic photovoltaic devices and organic bipolar transistors.[1–5] Crystalline organic/organic (O/O) heterostructures have drawn much attention recently for their promising potential application in nanoelectronics and novel functional organic devices, especially in optoelectronic devices, molecular chips and nanocircuits.[6–9] The heterostructure film's crystalline ordering and interface have been proven to be critical factors for the determination of the electronic structure and charge transport behavior.[10–17] However, compared with well-developed inorganic heterostructure engineering, crystalline organic heterostructures are still at the beginning level.[18,19] The reasons for the restriction in development are attributed to 1) difficulties in controlling ordered growth of molecules on another crystalline organic layer to realize a high mobility medium and 2) difficulties in adjusting O/O interfacial electronic structure to control carriers' transport in crystalline systems. Therefore, the understanding of the structure relationship in O/O systems and the interfacial electronic properties are of great importance in developing crystal engineering of organic heterostructures. In this paper, we construct a series of highly ordered O/O heterostructures using four different rod-like molecules and vanadyl phthalocyanine (VOPc) (**Figure 1**) to systematically investigate the interfacial crystal structure, electronic structure, and demonstrate an important clue to combine molecule design of conjugated oligomer with crystal growth engineering to tailor organic heterostructures devices with different performance.

Weak epitaxy growth (WEG) technique was used to form the crystalline heterostructure, in which the four rod-like molecules act as inducing layer to epitaxially grow VOPc film.[20,21] The four rod-like molecules, *para*-sexiphenyl (*p*-6P), 2,5-bis (4-biphenylyl) bithiophene (BP2T), 2,5-bis(4-biphenylyl)-thieno[3,2-b]thiophene (BPTT) and 2,7-bis(4-biphenylyl)-phenanthrene (BPPh), are a kind of conjugated oligomers with the same ending biphenyl group but different central group (Figure 1).[22,23] Although the morphology of these rod-like molecular layers presents high similarity, the difference of their molecular structure results in apparently different epitaxial morphology of VOPc, which is owing to the difference in the lattice mismatch. On the other hand, the O/O interfacial electronic structure varied with the rod-like molecules and demonstrate different barrier for charge injection. The conjunct effect from morphology and electronic structure leads to diverse transport behavior in the organic thin film transistor based on these heterostructure.

L. Huang, C. Liu, Dr. H. Tian, Dr. J. Zhang, Prof. Y. Geng, Prof. D. Yan
State Key Laboratory of Polymer Physics and Chemistry
Changchun Institute of Applied Chemistry
Chinese Academy of Sciences
Changchun, 130022 P. R. China
E-mail: yandh@ciac.jl.cn
Dr. F. Zhu, U. Treske, M. Grobosch, Prof. M. Knupfer
Leibniz Institute of Solid State and Materials Research Dresden
Dresden 01069, Germany
E-mail: f.zhu@ifw-dresden.de

DOI: 10.1002/adfm.201200014

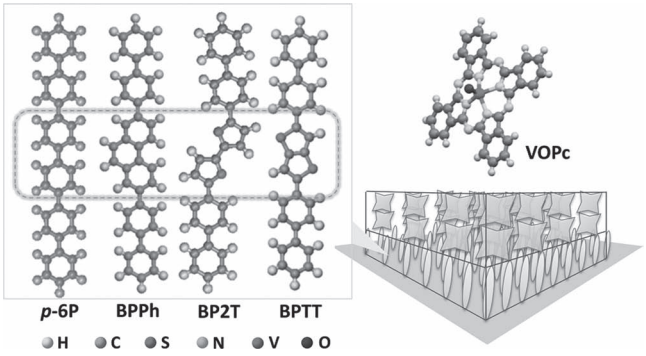

Figure 1. The heterostructure configuration and the molecular structure of *p*-6P, BPPh, BP2T, BPTT, and VOPc.

2. Results and Discussions

2.1. Rod-Like Molecules and Morphology of Films

Conjugated oligomers are an important sort of organic semiconductor molecules, of which the molecular groups can be easily designed to adjust the electronic properties. The four rod-like molecules we choose are composed of different central groups, which result in different crystal structure and electronic structure theoretically. In this part, firstly we fabricated high crystalline smooth layers of the four rod-like molecules on heated substrates. The growth process obeys the rules of diffusion limited aggregation (DLA).[27–29] Using the optimized conditions, all the four molecular films present large disc-like islands with compact coalescence, forming highly ordered, continuous and smooth film on the substrate. **Figure 2** is the typical AFM topographic images of 2.5 nm and 5 nm films grown on the SiO_2/Si substrate. The 2.5 nm film mainly contains monolayer domains while the 5 nm film is mainly composed of bilayer domains. The first layer (monolayer) of the four molecules always presents typical layer by layer growth fashion, in which the monolayer domains nucleate and grow on the substrate and finally coalesce with each other, while second layer domains only appear when the first layer almost cover the surface. This leads to smooth monolayer films as Figure 2a–d shows. The second layers of the four molecules except the *p*-6P remain in a typical layer-by-layer growth fashion. For the *p*-6P, a transition to island growth in the second layer and formation of a relatively rough surface is observed, which has been reported in previous work.[28] Apparently, the density of second layer domains is slightly larger for BPPh than others which might be attributed to the rigid of phenanthrene group. Nevertheless, the large domains and the smooth feature of the four molecular films render them good candidates for the growth of the upper layer in the heterostructure.

The structure properties of the four rod-like molecular films are critical for the heterostructure for they act as the inducing layer. **Figure 3** shows the two dimensional GIXRD patterns of the four rod-like molecular films. Besides the out-of-plane diffraction of (00*l*), the in-plane diffraction of (110) (20*l*) and (21*l*) can be clearly observed. Slight difference is observed for the

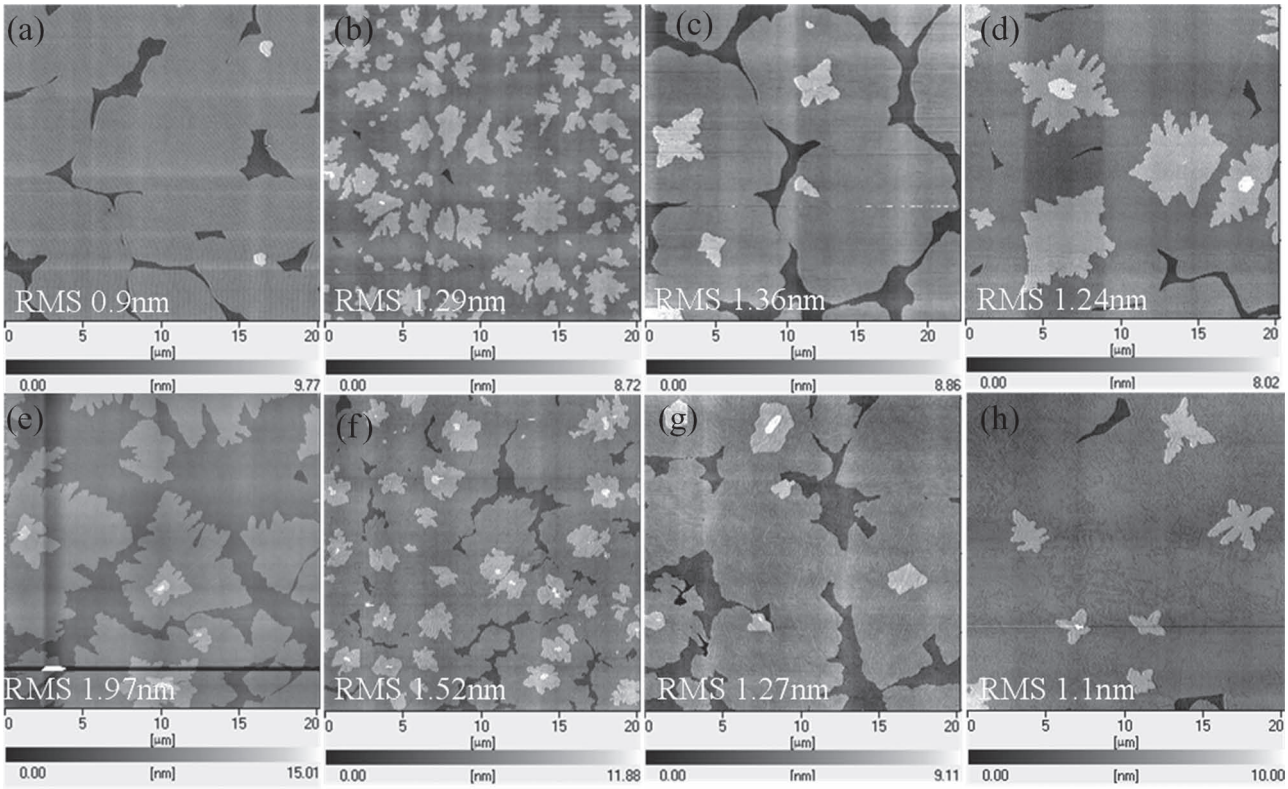

Figure 2. AFM topographic images of 2.5 nm (a–d) and 5 nm (e–h) film of the four molecules. a,e) *p*-6P, b,f) BPPh, c,g) BPTT, d,h) BP2T.

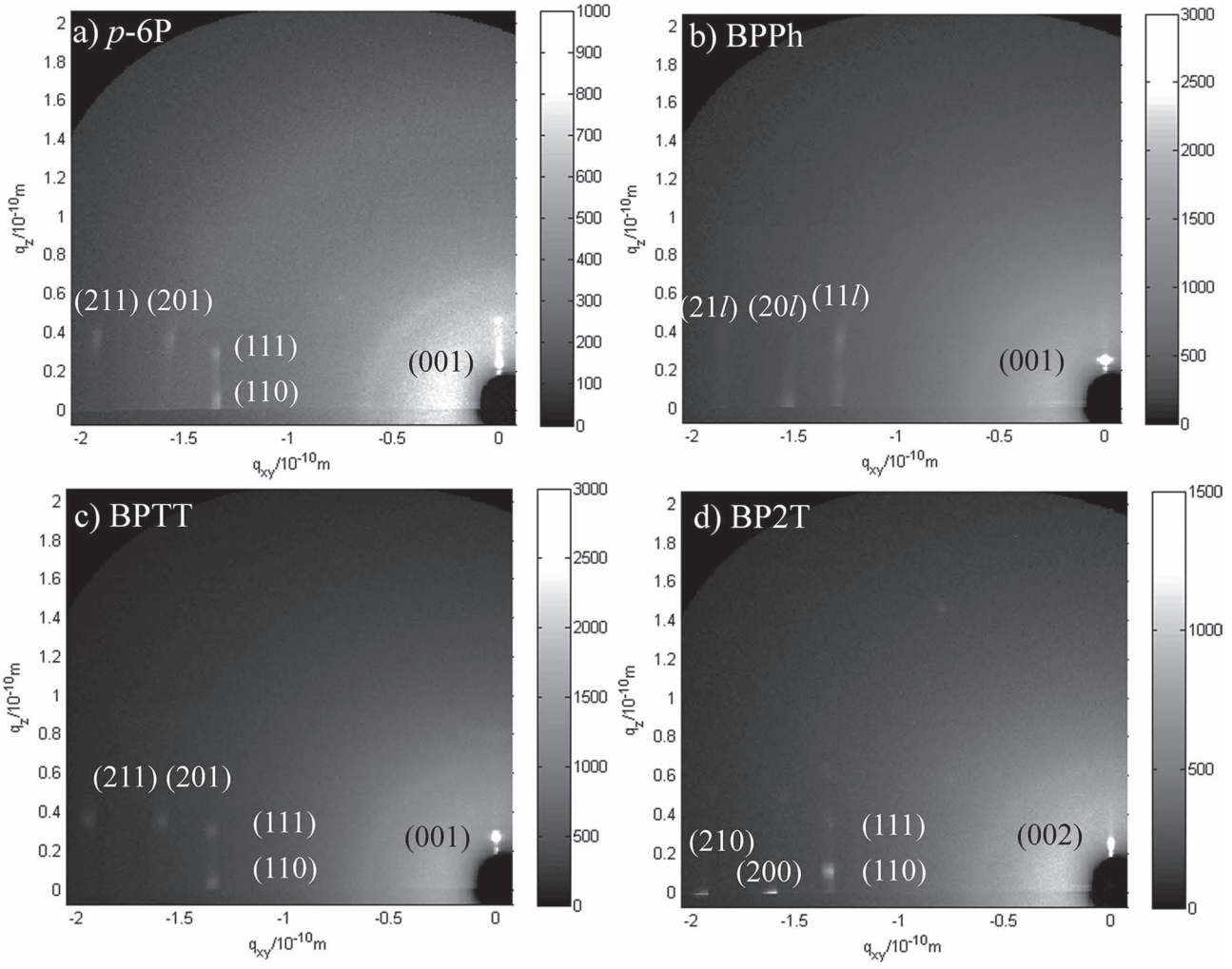

Figure 3. 2D-GIXRD images of a) *p*-6P, b) BPPh, c) BPTT, and d) BP2T films.

position and diffraction pattern of the four molecules. The *p*-6P and BPTT present strong diffraction of (201) and (211), while the BP2T and BPPh exhibit strong diffraction of (200) and (210) planes, which is originated from the various tilt angles of the four molecules relative to the substrate. According to the diffraction pattern and the position, the film structure parameters can be calculated. **Table 1** summarized the parameters of the four rod-like molecular films. All the film structures were ascribed to monoclinic or orthorhombic systems. In addition, the molecule is upright relative to the substrate according to the out-of-plane diffraction such as (00l), the *ab* plane is the exposure plane in the film surface. The GIXRD data reflect that the *ab* plane lattice parameters vary with the molecular structure. Compared to *p*-6P, the BPPh has a larger surface unit cell, while BPTT and BP2T expand in the *b* axis but shrink in the *a* axis, which results in a slightly smaller surface unit cell. Difference in the surface lattice parameters will influence the upper layer's growth. The field effect mobility of the four molecular films was measured for backup, which are at the scale of 0.02–0.07 cm^2/V s, relatively smaller than ordered phthalocyanines. The result is summarized in Table 1.

2.2. Morphology of Rod-Like Molecule/Nonplanar Phthalocyanine Organic Heterostructures

VOPc is a typical phthalocyanine organic semiconductor, which has high mobility and abundant photoelectronic properties.[21,30] A layer of VOPc is deposited on the above rod-like molecular film surfaces to form a series of VOPc/"rod" organic heterostructures. **Figure 4** shows the topographic images of 3 nm VOPc grown on the 2.5 nm (monolayer) and 5 nm (bilayer) rod-like molecular films. On the monolayer of all the rod-like molecules, VOPc forms typical pyramid-like crystal with laminated structure and presents typical island growth behavior. Crystals with several orientations distributed uniformly on each grain of the rod-like molecules, adjacent crystal grain coalesced compactly. However, VOPc presents great difference on the bilayer of different rod-like molecules. On the *p*-6P and BPPh bilayer, VOPc is characterized by a similar morphology to that on the monolayer with grain size smaller than 1 μm. But on BPTT and BP2T bilayer domains, as Figure 4g and h shows, VOPc formed laminated crystal grains larger than 2 μm accompanied with good coalescence behavior between adjacent domains.

Table 1. Lattice parameters of four rod-like molecular films and the corresponding HOMO and field effect mobility. Error bar of the lattice parameter is 0.02 Å.

Inducing layer	(200) [Å]	(010) [Å]	(110) [Å]	HOMO [eV]	Mobility [$cm^2 V^{-1} s^{-1}$]
p-6P	4.00	5.56	4.57	5.9	0.02
BPTT	3.84	5.63	4.54	5.46	0.07
BP2T	3.80	5.70	4.54	5.2	0.03
BPPh	3.99	5.90	4.74	6.07	0.03

Such a growth morphology is quite close to the situation of layer by layer growth, which is hard to realize for the nonplanar phthalocyanines. In order to gain insight into the film quality and difference, out-of-plane XRD was performed to determine the structure of VOPc films, as Figure S1 (Supporting Information) shows. On the four inducing layers, the WEG VOPc films all present a series of (0*k*0) diffraction, which are ascribed to (010), (020), and (030) of the phase II, respectively. These results supply clear evidence for the high order of the heterostructure films. On the other hand, the series of (0k0) diffraction reflect the VOPc molecules are upright relative to the substrate, while the π–π stacking direction is in plane, which is favorable for the charge carrier transport in the transistors.

Selected area electron diffraction (SAED) is performed to analyze the in-plane structure of the heterostructure. SAED patterns clearly demonstrate that VOPc films on BPTT and BP2T bilayer are quite different from that on *p*-6P and BPPh. **Figure 5**a,c show the SAED patterns of VOPc grown on *p*-6P and BPTT bilayer. For the VOPc/*p*-6P, besides the (001) zone diffraction of *p*-6P, the pattern contains four sets of diffraction of VOPc (Figure 5a). According to the diffraction spot of (-2-12) of VOPc, four sets of orientations of VOPc on one bilayer domain of *p*-6P were analysed. The reciprocal vector of $(-2-12)_{VOPc}$ plane is parallel to the a^* axis of *p*-6P for the orientation 1, and is parallel to the (110) of *p*-6P for the orientation 2, while it is parallel to the (210) of *p*-6P for the orientation 3. For the orientation 4, the reciprocal vector of $(-2-12)_{VOPc}$ plane forms an angle of 17° with the a^* axis of *p*-6P. In the packing pattern of the phase II, the VOPc molecular plane is nearly on the (-2-12) plane of VOPc. Hence in the four orientations, the VOPc molecular plane is also parallel to the corresponding directions of the *p*-6P, which is clearly demonstrated in the schematic diagram of VOPc packing on the inducing layer surface (**Figure 6**).

However, on the BPTT and BP2T bilayer, the diffraction pattern mainly presents two orientations of VOPc crystals, corresponding to the orientation 1 and 2 in the situation of *p*-6P. Referred the AFM results, we know that the morphology of VOPc on BP2T and BPTT is much better than that on *p*-6P and BPPh, which should be closely related with the in-plane orientation. In the schematic diagram of VOPc on inducing layers (Figure 6a,b), for the orientation 1 and 2 the VOPc molecules are parallel to the corresponding array in the inducing layer with some lattice axes coincidence with each other, indicative

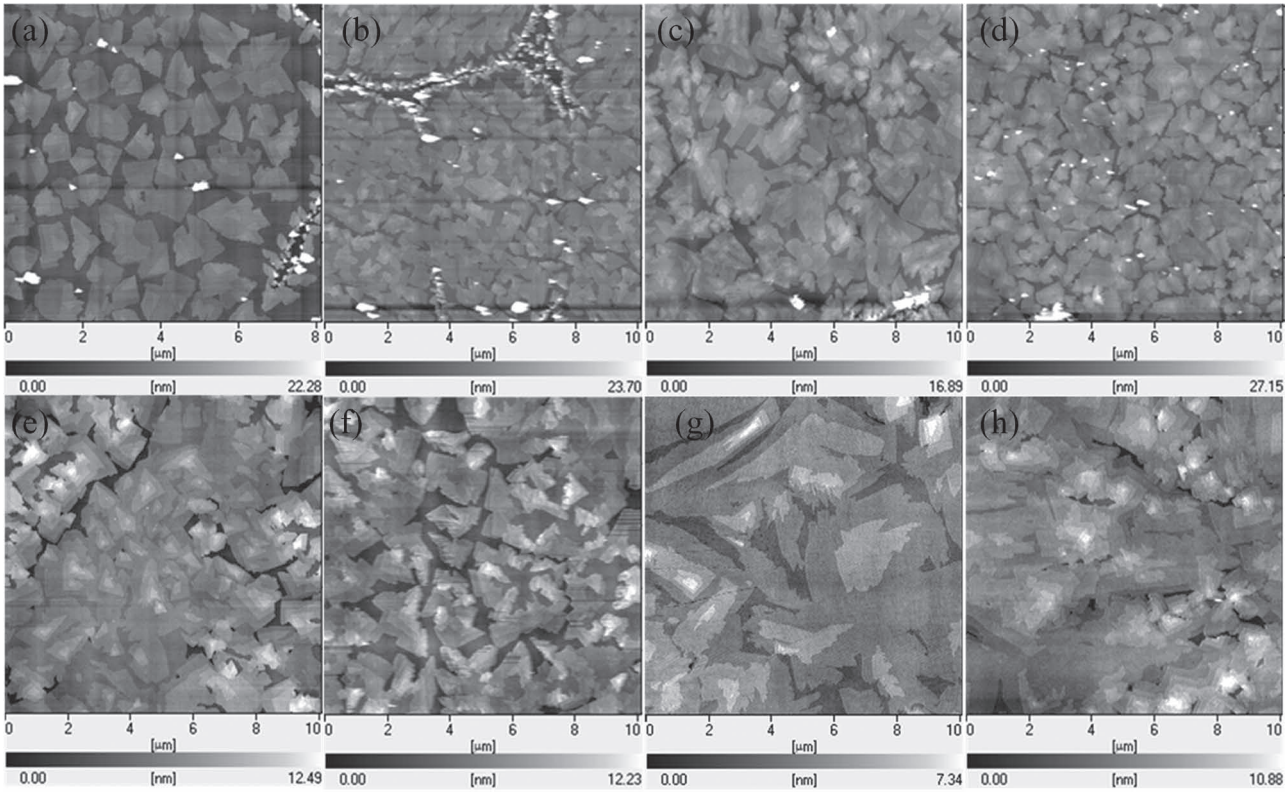

Figure 4. AFM topographic images of VOPc/"rod" molecular films, a) VOPc/*p*-6P(2.5 nm), b) VOPc/BPPh(2.5 nm), c) VOPc/BP2T(2.5 nm), d) VOPc/BPTT(2.5 nm), e) VOPc/*p*-6P(5 nm), f) VOPc/BPPh(5 nm), g) VOPc/BP2T(5 nm), and h) VOPc/BPTT(5 nm).

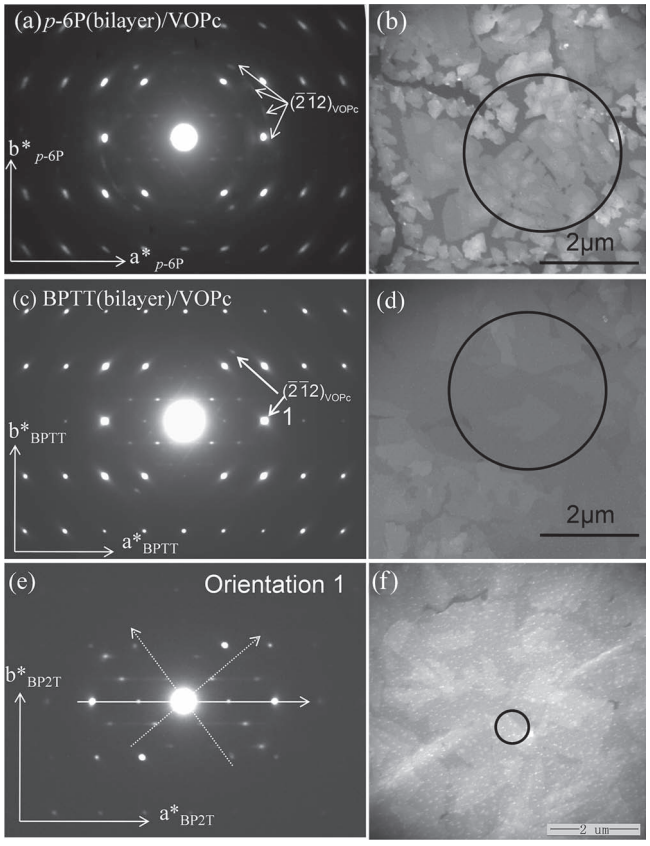

Figure 5. SAED patterns of a,b) VOPc/*p*-6P(bilayer), c,d) VOPc/BPTT(bilayer), and tilt SAED pattern of e,f) VOPc/BP2T(bilayer).

of commensurate epitaxy possibility. For further confirming the epitaxy relationship of the VOPc on BP2T or BPTT, the tilt SAED mode was carried out to measure. Let the incidence direction nearly parallel to the [010] direction of VOPc, the [010] zone of VOPc can be clearly observed. Figure 5c shows the SAED pattern of orientation 1. The diffraction pattern of VOPc is much clearer than that of [1-20] zone and exhibit strong diffraction intensity of (h00), (0k0) and (-101) planes. The lattice relationship of VOPc and the BP2T can be clearly inferred from the pattern. The (-101)VOPc//(100)BP2T, and lattice plane coincidence was observed on this direction, proving the commensurate epitaxy between VOPc and BP2T or BPTT. Such epitaxy is favorable for the large size grain and smooth film growth.

The epitaxy growth morphology is critically related with the lattice mismatch between the inducing layer and the epitaxial VOPc layer. Owing to the different central groups, the four inducing layers possess similar crystal stacking, but with different lattice parameters. Thus, we can infer the lattice mismatch between VOPc and the rod-like molecules might account for the structure difference and the various epitaxy growth behaviors. **Figure 7** shows the lattice mismatch between the four rod-like molecules and the VOPc at the situation of the orientation 1 and orientation 2, which are the main orientations and also the favorable orientations in the system as discussed below. The lattice mismatch is mainly lower than 5% for the VOPc/BPTT and VOPc/BP2T, but up to about 10% for the VOPc/*p*-6P and VOPc/BPPh. Hence, in the VOPc/BP2T or VOPc/BPTT heterostructure, small lattice mismatch leads to a nearly layer by layer growth behavior and less orientations, which are favorable morphology for the charge transport in transistor. The similar morphology of the VOPc is related with the less ordered and looser structure of the monolayer film caused by the stress on the bare SiO_2/Si surface.[29] In other words, different central group of "rod" results in different lattice mismatch in the series VOPc/"rod" heterostructure, and lead to the difference in their morphology, from a continuous and layered film with large grains to a discontinuous and island grown films with small grains.

2.3. Electronic Structure of the Rod-Like Molecule/Nonplanar Phthalocyanine Heterostructures

The central groups in rod-like molecules will have an influence on the molecular energy level and electron distribution. As a result, the interfacial electronic structure due to the "rods" could also be influenced. In this part, photoemission spectroscopy (PES) is introduced to characterize the interfacial electronic structure of the four VOPc/"rods". From the ultraviolet photoelectron spectroscopy (UPS) spectra, the molecular orbital alignment, the work function Φ, the interface dipole Δ, the

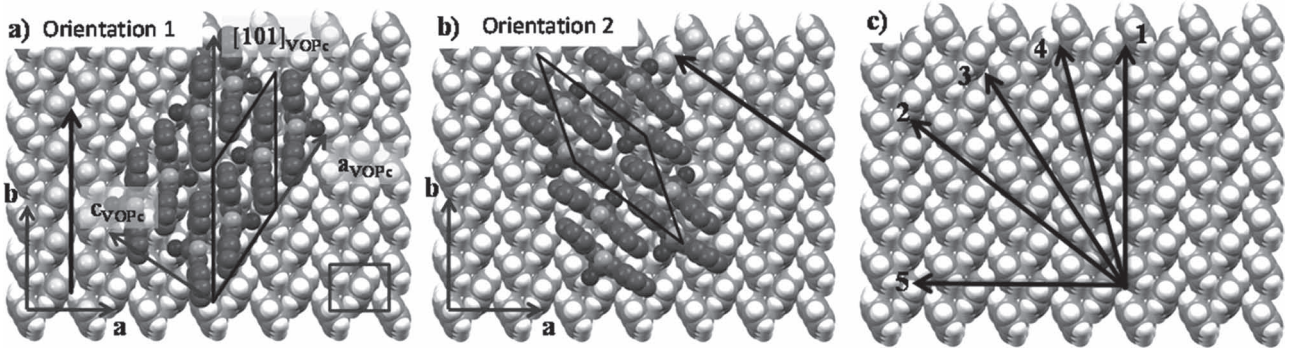

Figure 6. Schematic packing diagrams of VOPc on rod-like molecules: a) orientation 1, b) orientation 2, and c) the schematic diagram of the five orientations of VOPc on *p*-6P.

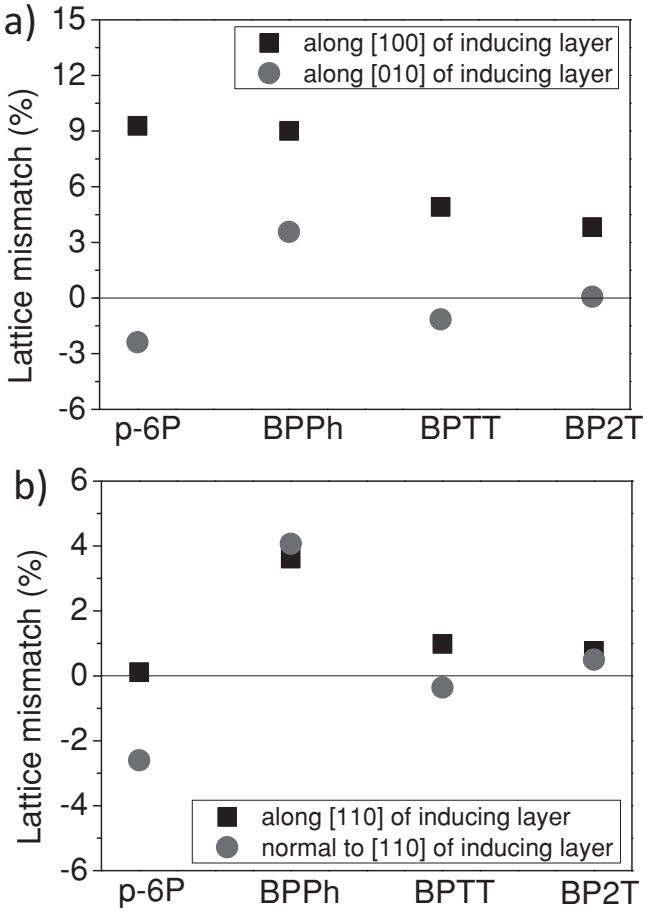

Figure 7. Lattice mismatch between VOPc and four rod molecular films. a) orientation 1 and b) orientation 2. The error is 0.2% according to the calculation and the lattice parameters.

ionization potential (IP) and the hole injection barriers (HIB) can be extracted. The details of the analysis of UPS spectra and parameters have been thoroughly introduced in several reviews.[13,31,32] **Figure 8** illustrates the valence-band PES results taken for the VOPc/*p*-6P, VOPc/BPPh, VOPc/BPTT and VOPc/BP2T. For comparison, the intensity was normalized to the height of the most intense spectral feature. The Fermi level of each system is pinned to the work function of the corresponding Si substrate. As shown in Figure 8a, the major parameters (highest occupied molecular orbital (HOMO) onset, the high binding energy cutoff (HBEC) and their shifts) can be determined from the clear spectra. The X-ray photoemission (XPS) spectra were also carried out to investigate the evolution of core levels in the heterostructures. The spectral features of O1s, N1s, $V2p_{3/2}$ (of VOPc) and S2p (of BPTT and BP2T) core levels do not show obvious changes, which means the change in core levels is evidently lower than the XPS measurement error (0.35 eV). Furthermore, there is no new peak appearing during the growth process, which clearly indicates the interaction between rod-like molecules and VOPc is of physisorption character. The results from the photoemission measurements are summarized (Figure S2 in Supporting Information). The corresponding interfacial electronic structure can be derived in a schematic energy level diagram (**Figure 9**).

Besides dipoles existing at the interfaces of the four systems, we observed a gradual energy shift of both HBEC and HOMO onset in a 5 nm range during the deposition of VOPc in the VOPc/BPTT and VOPc/BP2T system. Although the shift value is comparable to the resolution of UPS, we suggest this shift indicates a weak energy level bending instead of a complete interfacial dipole. There are several reasons: 1) The S elements in BPTT and BP2T have the ability of withdrawing electrons in the heterojunction systems. This is similar to the case of F elements in F_{16}CuPc/CuPc, in which the charge transfer and band bending is confirmed.[33] 2) The energy level bending at the interface of CuPc/BP2T is already confirmed by PES experiment, which is also a P/P type organic heterostructure.[26] Generally speaking, the energy level alignment will determine the charge transport across the interface or along the interface. After the analysis of interfacial energy alignment, we clearly observe that the HIBs in the four systems have quite different values. For VOPc/BPTT and VOPc/BP2T, the HIB between VOPc and inducing layer is nearly equal to zero. Consequently, holes can easily flow in two directions, either from inducing layer to VOPc or vice versa. For VOPc/*p*-6P and VOPc/BPPh, the HIB between VOPc and inducing layer is 0.60 eV and 0.50 eV, respectively, which can block the holes effectively when flowing from VOPc to *p*-6P or BPPh.

2.4. Transistor Performance of Rod-Like Molecule/Nonplanar Phthalocyanine Organic Heterostructures

Utilizing the four molecules as the inducing layer (2.5–5 nm) and VOPc (20 nm) as the active layer, we fabricated heterostructure transistors of top contact bottom gate configuration. **Figure 10** shows the typical transfer characteristics with V_{SD} of –50 V, of which the transistor is in the saturation region. For the *p*-6P/VOPc and BPPh/VOPc transistors, independent of 2.5 nm or 5 nm thickness of the inducing layer, typical p-type transport behaviors were measured. The saturated field-effect mobility is larger than 1.5 cm^2/Vs along the whole gate voltage with a threshold voltage less than –10 V and current on/off ratio of 10^5. However, the performance of BP2T/VOPc and BPTT/VOPc is far away from what would be expected from their morphology. The p type mobility reaches 1.5 cm^2/Vs only at the low gate voltage scale with the 2.5 nm inducing layer for both BPTT and BP2T. At high gate voltage, the mobility sharply decreases to the scale of 0.3–0.4 cm^2/Vs. As the BPTT or BP2T increase to 5 nm (most contains bilayer domains), the mobility was lower than 0.3 cm^2/Vs along the whole gate voltage scale, though the morphology of VOPc is quite good in this case. For the BP2T, a mobility of 0.08 cm^2/Vs was present which is close to the mobility of BP2T films. Figure S3 and Figure S4 show the detailed output and transfer characteristics of the series of transistors, the significant decreased performance of transistors based on 5 nm BPTT and BP2T can be clearly observed from their output characteristics, where the I_D are no more than 30 μA but the high mobility transistor is larger than 200 μA at the same condition. Some of the heterostructure transistors

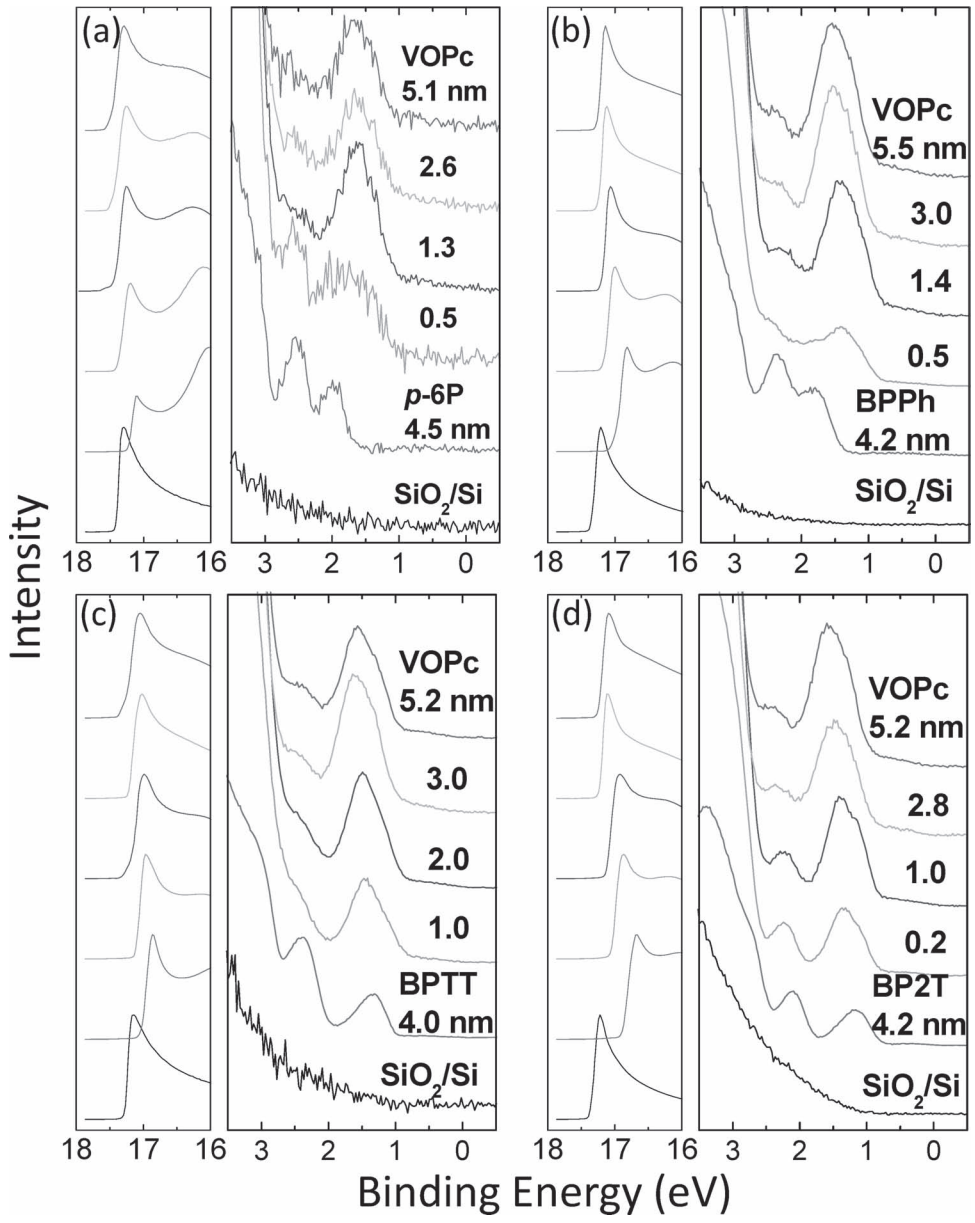

Figure 8. Evolution of the secondary electron cutoff and the HOMO region of the valence band PES spectra of a) VOPc/*p*-6P, b) VOPc/BPPh, c) VOPc/BPTT, and d) VOPc/BP2T.

also present ambipolar property. **Table 2** summarizes the performance of the VOPc/"rod" heterostructure transistors.

2.5. Discussions

The four transistors are characterized by hole transport behavior, and the charge transport behavior was demonstrated with the transfer characteristic curves. The performances of thin-film transistors exhibit large differences in the four systems. So we need to trace the major factors and how they influence the device performance. For the transistors, the film morphology and interface properties have been widely proved to be the primary factors determining the mobility. From the section 2.2 and 2.4 we know, although high crystalline heterostructure films form in the four systems, owing to the difference in growth behavior and mismatch of crystal lattice, VOPc films on the BPTT and BP2T possessed large grain, continuous and less grain boundary morphologies which is supposed to present better performance than that on *p*-6P and BPPh. However, their transistors hardly present high mobility of the highly ordered VOPc film. As we know, under the gate bias, the working channel of OTFT is mainly at the scope of 2 nm near the organic/substrate interface.[34,35] The four inducing layers

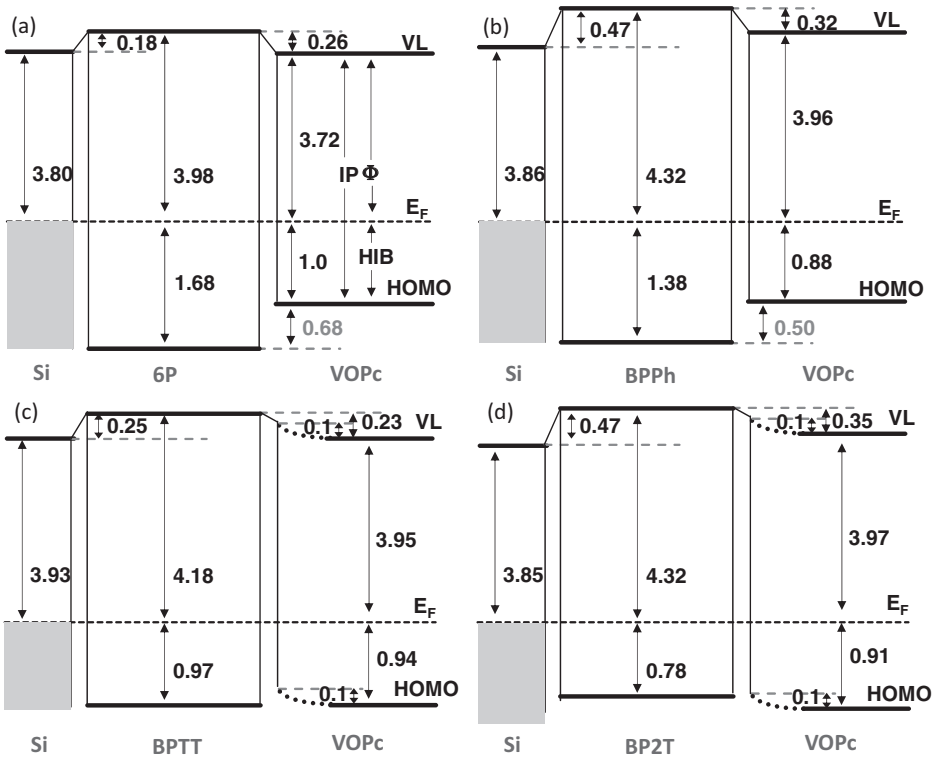

Figure 9. Schematic energy level diagrams of the crystalline heterostructure of a) VOPc/*p*-6P, b) VOPc/BPPh, c) VOPc/BPTT, and d) VOPc/BP2T. Energy values are in unit of electron volt (eV).

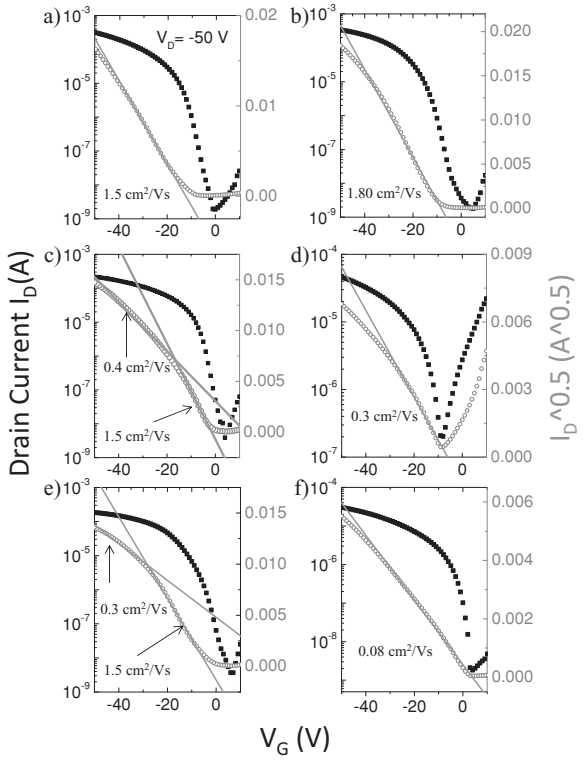

Figure 10. Transfer characteristics of VOPc/"rod" molecule heterstructure transistor, a) *p*-6P (2.5 nm)/VOPc, b) BPPh(2.5 nm)/VOPc, c) BPTT(2.5 nm)/VOPc, d) BPTT(5 nm)/VOPc, e) BP2T(2.5 nm)/VOPc, and f) BP2T(5 nm)/VOPc.

are p-type semiconductor layers, which present mobilities at the magnitude of 10^{-2} cm^2/Vs. Therefore, once charge carries injected in the inducing layer, they can act as the active layer in the transistor. The final performance might decrease owing to the relative low mobility of inducing layer compared with the VOPc. According to the PES results, for the BPPh/VOPc and *p*-6P/VOPc layer, the HIB is up to 0.5 eV, which is efficient enough to block the hole injecting from VOPc to the inducing layer. So in this case, the charge transport channel formed only at the VOPc layer in the transistor and then the mobility of the devices is completely accounted by the VOPc layer, hence high mobility was observed as **Figure 11**a shows. However, considering the energy level bending, the HIB between VOPc and

Table 2. Mobility, threshold voltage, and current on/off ratio of the series of rod/VOPc heterostructure based field-effect transistors.

Film	Mobility [cm^2/Vs]	V_{th} [V]	I_{on}/I_{off}
p-6P/VOPc	1.0 to 2.0	–8 to –12	10^5
BPPh/VOPc	1.0 to 2.2	–10 to –1	10^5
BPTT(2.5 nm)/OPc	0.4 (1.0 to 1.5)	–2 to –5	10^5
BPTT(5 nm)/VOPc[a)]	0.3	–8 to –12	10^3
BP2T(2.5 nm)/VOPc	0.3 (1.0 to 1.5)	–2 to –5	10^5
BP2T(5 nm)/VOPc	0.08	2 to –2	10^5

[a)]Ambipolar property was obviously observed for this system.

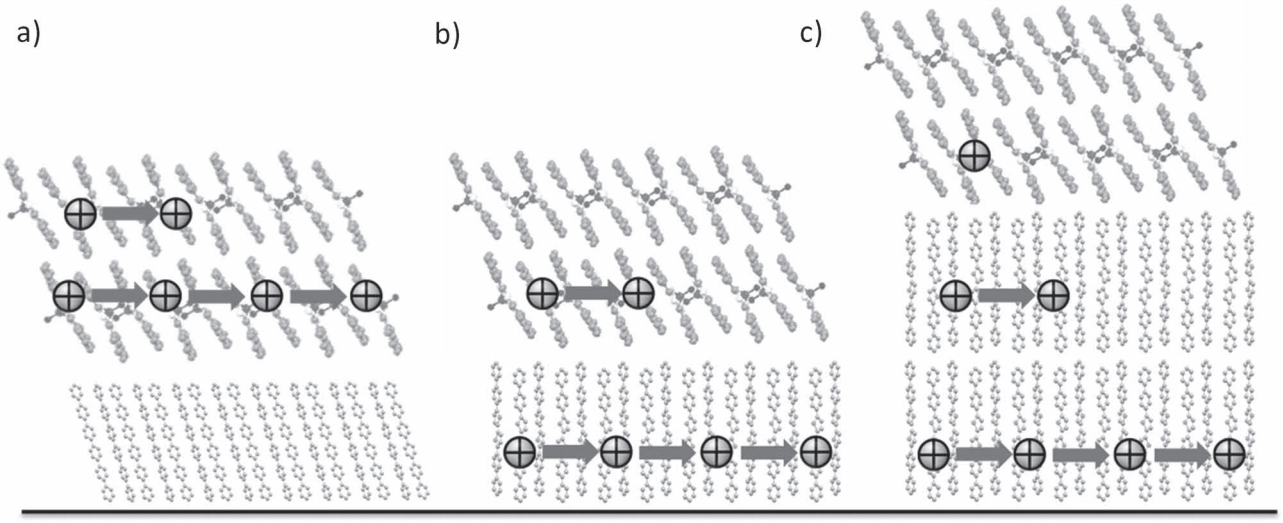

Figure 11. Schematic diagram of charge transport channel in the VOPc/"rod" hereorstructure transistor: a) VOPc/*p*-6P or BPPh, b) VOPc/BP2T or BPTT monolayer, and c) VOPc/BP2T or BPTT bilayer.

BP2T or BPTT is nearly equal to zero. In this case, the holes can easily inject from the VOPc layer into the inducing layer under the gate bias. The holes will have a wider scope of distribution under low gate bias than that under high bias.[36] So the holes will have different mobility if spread in VOPc or inducing layer. This is reflected by the two obvious regions existing in transfer characteristics of VOPc/BP2T(2.5 nm) and VOPc/BPTT(2.5 nm). The motilities shift from more than 1 cm^2/Vs to about 0.3 cm^2/Vs with increasing the gate voltage due to the holes' effectively injection cross the interface. For a thicker inducing layer (5 nm), most of the working channel is located at the inducing layer, so the TFT's mobility represent the transport in BP2T or BPTT layer (Figure 11b,c). These also represent the ascendant charge transport in the direction perpendicular to interface, which are beneficial for photovoltaic devices.

3. Conclusions

In this work, we systemically investigate several aspects of a series of crystalline organic heterostructures formed by VOPc and four rod-like molecules, e.g. crystal structure, epitaxial relationship, electronic structure, charge transport behavior and performance of OTFTs. Although the central groups are different, the rod-like molecules present a layer by layer growth and form continuous, smooth films with large size single-crystal domains. The upper VOPc layer present crystalline morphology varied with the central groups in "rods": discontinuous island growth, small size domains on *p*-6P and BPPh; continuous layered growth, large size domain on BP2T and BPTT. These variations originate from the distinct differences of lattice mismatch in the four systems. At the same time, the alignments of interfacial electronic levels and hole injection barrier at VOPc/rod-like interfaces also are dependent on the central groups of the four rod-like molecules. Owing to the above properties, the transistors present diverse performance and field-effect mobility. These results indicate high mobility vanadyl phthalocyanine and other disk-like molecules heterojunction films with different charge transport characteristics and crystal structures can be tailored through selecting rod-like molecules with different central groups, without losing high crystallinity. Combing with molecule design from chemists, more and more functional crystalline molecular films can be fabricated and multiple properties can be integrated in tailored crystal systems, e.g., optical waveguide, photoelectric sensor. This work illustrates the novel concept of crystalline solid-state engineering of organic semiconductors is very hopeful to be realized in near future.

Experimental Section

Materials and Film Growth: The rod-like molecules (*p*-6P, BP2T, BPTT, BPPh) were synthesized according to references.[22,24,25] The vanadyl phthalocyanine (VOPc) was purchased from Aldrich. All the materials were purified twice by gradient thermal sublimation prior to deposition. Highly doped n-type silicon wafers with thermally grown SiO_2 (300 nm, capacitance per unit area (*Ci*):10 nF cm^{-2}) were used as the substrate. The rod-like molecules with different thicknesses were directly deposited on the pre-cleaned SiO_2/Si substrate. Vanadyl phthalocyanine was then deposited on the rod-like molecular layer to form the organic heterostructure films. During the deposition, the substrate temperature was kept at 150–160 °C (for different rod-like molecules, the temperature is varied slightly), the deposition rate is at 1 nm per minute and the pressure is at 10^{-4}–10^{-5} Pa.

Film Characterization: The film morphologies were imaged by a SPI 3800/SPA 300HV atomic force microscope (Seiko Instruments Inc., Japan) with tapping mode. The selected area electron diffraction was performed by a JEOL JEM-1011 transmission electron microscope operated at 100 kV. Dark field was used for experiments to provide weaker-intensity beam and high contrast. The 2D-GIXRD measurements were carried out at BL14B1 in Shanghai Synchrotron Radiation Facility (SSRF) with a incidence wavelength of 1.24 Å.

The interfacial electronic structure of each "rod"/VOPc system is obtained from photoemission spectroscopy measurement during the

WEG process using a commercial PHOIBOS-150 (SPECS) ultrahigh vacuum (UHV) surface analysis system, which is equipped with a He-discharge lamp and a monochromatic Al Kα source providing photons with 21.22 eV for UPS (ultraviolet photoemission spectroscopy) and 1486.6 eV for XPS (X-ray photoemission spectroscopy), respectively. The total energy resolution of the spectrometer is about 0.1 eV (UPS) and 0.35 eV (XPS). For UPS the samples were measured under a bias of 7 V. For XPS the energy scale was calibrated to reproduce the binding energy of $Au4f_{7/2}$ (84.0 eV). A cleaned n-type Si wafer with a native oxide layer on top was used as substrate, which can guarantee the conductivity of the substrate for PES measurement and the smooth surface for WEG. Due to the high background vacuum (about 10^{-8} Pa), the substrate's temperature condition is optimized to 90–100 °C for taking advantage of the weak epitaxy growth condition. The experimental details are described in the references.[23,26]

OTFT Fabrication and Characterization: The gold contacts were thermally evaporated on the pre-fabricated film surface through shadow masks to form bottom-gate top-contact transistors with a channel width (W) and length (L) of 6000 µm and 200 µm, respectively. The current-voltage characteristics of the devices were measured with two Keithley 236 source-measurement units under ambient conditions at room temperature.

Supporting Information

Supporting Information is available from the Wiley Online Library or from the author.

Acknowledgements

This work was supported by the National Natural Science Foundation of China (50803063), the National Basic Research Program (2009CB939702) and the German Science Foundation (DFG, KN393/9). The authors thank beam line BL14B1 (Shanghai Synchrotron Radiation Facility) for providing the beam time.

Received: January 3, 2012
Revised: May 2, 2012
Published online: June 20, 2012

[1] C. W. Tang, *Appl. Phys. Lett.* **1986**, *48*, 183.
[2] C. W. Tang, S. A. VanSlyke, *Appl. Phys. Lett.* **1987**, *51*, 913.
[3] A. Dodabalapur, H. E. Katz, L. Torsi, R. C. Haddon, *Science* **1995**, *269*, 1560.
[4] J. J. M. Halls, C. A. Walsh, N. C. Greenham, E. A. Marseglia, R. H. Friend, S. C. Moratti, A. B. Holmes, *Nature* **1995**, *376*, 498.
[5] G. Yu, J. Gao, J. C. Hummelen, F. Wudl, A. J. Heeger, *Science* **1995**, *270*, 1789.
[6] G. Koller, S. Berkebile, J. R. Krenn, F. P. Netzer, M. Oehzelt, T. Haber, R. Resel, M. G. Ramsey, *Nano Lett.* **2006**, *6*, 1207.
[7] M. Campione, L. Raimondo, A. Sassella, *J. Phys. Chem. C* **2007**, *111*, 19009.
[8] F. Zhu, K. Lou, L. Z. Huang, J. B. Yang, J. D. Zhang, H. B. Wang, Y. H. Geng, D. H. Yan, *Appl. Phys. Lett.* **2009**, 95.
[9] Y. Zhang, H. Dong, Q. Tang, S. Ferdous, F. Liu, S. C. B. Mannsfeld, W. Hu, A. L. Briseno, *J. Am. Chem. Soc.* **2010**, *132*, 11580.
[10] W. Chen, S. Chen, H. Huang, D. C. Qi, X. Y. Gao, A. T. S. Wee, *Appl. Phys. Lett.* **2008**, *92*, 063308.
[11] W. Chen, S. Chen, Y. L. Huang, H. Huang, D. C. Qi, X. Y. Gao, J. Ma, A. T. S. Wee, *J. Appl. Phys.* **2009**, *106*, 064910.
[12] Z. Li, J. Du, Q. Tang, F. Wang, J.-B. Xu, J. C. Yu, Q. Miao, *Adv. Mater.* **2010**, *22*, 3242.
[13] D. Cahen, A. Kahn, *Adv. Mater.* **2003**, *15*, 271.
[14] W. Chen, H. Huang, S. Chen, Y. L. Huang, X. Y. Gao, A. T. S. Wee, *Chem. Mater.* **2008**, *20*, 7017.
[15] Y. L. Gao, H. J. Ding, H. B. Wang, D. H. Yan, *Appl. Phys. Lett.* **2007**, *91*, 142114.
[16] J. W. Shi, H. B. Wang, D. Song, H. Tian, Y. H. Geng, D. H. Yan, *Adv. Funct. Mater.* **2007**, *17*, 397.
[17] M. Mas-Torrent, C. Rovira, *Chem. Rev.* **2011**, *111*, 4833.
[18] Y. Zhang, E. Barrena, X. Zhang, A. Turak, F. Maye, H. Dosch, *J. Phys. Chem. C* **2010**, *114*, 13752.
[19] R. Lunt, K. Sun, M. Kröger, J. Benziger, S. Forrest, *Phys. Rev. B* **2011**, *83*, 064114.
[20] H. Wang, F. Zhu, J. Yang, Y. Geng, D. Yan, *Adv. Mater.* **2007**, *19*, 2168.
[21] H. B. Wang, D. Song, J. L. Yang, B. Yu, Y. H. Geng, D. H. Yan, *Appl. Phys. Lett.* **2007**, *90*, 253510.
[22] L. Huang, C. Liu, X. Qiao, H. Tian, Y. Geng, D. Yan, *Adv. Mater.* **2011**, *23*, 3455.
[23] F. Zhu, M. Grobosch, U. Treske, L. Huang, W. Chen, J. Yang, D. Yan, M. Knupfer, *ACS Appl. Mater. Interfaces* **2011**, *3*, 2195.
[24] F. Garnier, G. Horowitz, X. Z. Peng, D. Fichou, *Synth. Met.* **1991**, *45*, 163.
[25] S. Hotta, H. Kimura, S. A. Lee, T. Tamaki, *J. Heterocyclic. Chem.* **2000**, *37*, 281.
[26] F. Zhu, M. Grobosch, U. Treske, M. Knupfer, L. Huang, S. Ji, D. Yan, *Appl. Phys. Lett.* **2011**, *98*, 203303.
[27] F. Heringdorf, M. C. Reuter, R. M. Tromp, *Nature* **2001**, *412*, 517.
[28] J. L. Yang, T. Wang, H. B. Wang, F. Zhu, G. Li, D. H. Yan, *J. Phys. Chem. B* **2008**, *112*, 7821.
[29] L. Z. Huang, C. F. Liu, B. Yu, J. D. Zhang, Y. H. Geng, D. H. Yan, *J. Phys. Chem. B* **2010**, *114*, 4821.
[30] L. Li, Q. Tang, H. Li, W. Hu, *J. Phys. Chem. B* **2008**, *112*, 10405.
[31] H. Ishii, K. Sugiyama, E. Ito, a. K. Seki, *Adv. Mater.* **1999**, *11*, 605.
[32] S. Braun, W. R. Salaneck, M. Fahlman, *Adv. Mater.* **2009**, *21*, 1450.
[33] K. M. Lau, J. X. Tang, H. Y. Sun, C. S. Lee, S. T. Lee, D. Yan, *Appl. Phys. Lett.* **2006**, *88*, 173513.
[34] F. Dinelli, M. Murgia, P. Levy, M. Cavallini, F. Biscarini, D. M. de Leeuw, *Phys. Rev. Lett.* **2004**, *92*, 116802.
[35] G. Horowitz, *J. Mater. Res.* **2004**, *19*, 1946.
[36] D. Braga, G. Horowitz, *Adv. Mater.* **2009**, *21*, 1473.